LASER CLEANING OF GREY CAST IRON AUTOMOTIVE BRAKE DISC: RUST REMOVAL AND IMPROVEMENT IN SURFACE INTEGRITY

Y. F OGBEKENE[1], P. SHUKLA[1*], Y. ZHANG[2], X. SHEN[1], S. PRABHAKARAN[3], S. KALAINATHAN[3], K. GULIA[4], AND J. LAWRENCE[1]

[1*]*School of Mechanical, Aerospace and Automotive Engineering, Coventry University, Priory Street, Coventry, CV1 5FB, United Kingdom.*

[2] *University of Lincoln, Brayford Way, Brayford Pool, Lincoln, LN6 7TS, United Kingdom*

[3]*Centre for Crystal Growth, Department of Physics, School of Advanced Sciences, Vellore Institute of Technology, Vellore, 632014, Tamilnadu, India.*

[4]*Faculty of Science and Engineering, School of Engineering, University of Wolverhampton, Priorslee, Telford TF2 9NN, United Kingdom*

[1*]Corresponding Author: ac5190@coventry.ac.uk

ABSTRACT

There is a great need for removal of rust and surface damage from corroded engineering parts, and this enables the retention of strength and increased longevity of metals and alloys in general. The use of lasers for cleaning, polishing and ablation has proven to be effective and promising over-time. This research focused on a parametric study of laser cleaning of a corroded grey cast iron brake disc. A continuous wave Rofin Multi-scan CO_2 laser having a wavelength of 10.6µm was used for the study. A systematic approach was employed for the experiments, where one parameter is changed, while other parameters were constant. Additional effects of laser cleaning were predicted by a Gaussian process regression approach. The results revealed that the best parameters which cleanly removed the rust were 60W of laser power, 900mm/s transverse speed, and a spot size of 722µm. The enhancement of surface microhardness of laser cleaned specimen was 37% compare to the rusted specimen surface. The roughness of the laser cleaned surface was 1.29µm while the rusted surface comprised of 55.45µm (Ra). Microstructural analysis showed a presence of randomly distributed graphite flakes surrounded by a pearlitic matrix containing ferrite and cementite after laser cleaning. This was similar to that of the un-rusted surface. The hardness, roughness and microstructural content were in close relation with the respective properties of the un-

rusted automotive brake disc. This showed that the mechanical and physical properties of the brake disc were not altered negatively during the laser cleaning process. Implementation of the laser-cleaning technique in automotive and manufacturing industries should be embraced as it provides a faster, safer and cheaper way of enhancing the surface integrity of components and also makes way for other surface enhancement methodologies to be applied such as blast cleaning or laser shock cleaning for inducing extra strength.

Keywords: Cast Iron; Laser Cleaning; Laser Polishing; Ablation; Corrosion; Surface integrity; Brake Disc.

1 INTRODUCTION

1.1 Overview

Rusting is an unavoidable natural phenomenon that has been a global menace for ages. This has caused so much damage over time ranging from crude farm tools to valuable historical artefacts, modern-day industrial, engineering and domestic parts made from metals and alloys. The annual cost of corrosion worldwide is $2.2 trillion which is over 3% of the world GDP [1]. This brings the need to counter/remove rust. Over the years, rust removal has evolved from a more primitive technique that includes scrubbing, the use of white vinegar, salt, lime, baking soda to the use of chemicals and other modern rust removal techniques [2]. These techniques are less effective to consume both time and energy, and there is an increasing need to use effective and quicker ways of removing rust which has led to the use of industrial lasers.

Metals and alloys are used in our day-to-day activities be it domestic, automobile or industrial. These metals and alloys are constantly exposed to the surrounding which acts chemically on it causing degradation of its part leading to corrosion [3]. Corrosion is a chemical or electrochemical reaction that causes the disintegration of an engineering material [4]. Rusting is specific to iron and its alloys [5]. It occurs when iron reacts with moist air or water to form iron oxide [6]. Therefore, rusting leads to a decrease in the performance, life span and failure of engineering materials [7], since rust affects irons and its alloys in which cast iron falls into that subset of metals. A brake disc made of cast iron will be used as a case study with the aim of the investigation was to obtain the optimal laser parameters that are most suitable for the removal of rust from metals and alloys.

1.2 Research Background

Laser cleaning involves the removal of rust/corrosion from the surface of the metal [8]. It involves the removal of debris, contaminant and impurities (silicon or rubber) by laser irradiation [9]. Variety of industrial laser cleaning applications are done using a pulsed fibre laser with high repetition rate, short pulse and high peak power [10]. During the process of laser cleaning, it is necessary that the physical and mechanical properties of the base metal were not modified [11].

Similar research on laser cleaning of corroded layers due to environmental pollution on metallic objects showed that the rate of laser ablation increased with increasing laser fluence [12]. They suggested the fluence should be within the ablation domain, that is greater than the vaporisation threshold, but less than the saturated domain [12]. The base metal is affected once it reaches the saturated domain [13]. Zhenyong *et al.* [14] gave a similar viewpoint to Siatou *et. al* [12], but argues that the cleaning efficiency of a pulsed Nd: YAG laser is better than that of the CO_2 laser. They further explained that the high laser absorbency of rust particles plays a vital role in the cleaning mechanism [15]. Irrespective of the preferred use of pulsed lasers over continuous wave CO_2 lasers for cleaning, a successful rust removal process has been carried out using the CO_2 laser [16]. Also, proper laser cleaning does not damage the metal substrate nor negatively alter its mechanical properties and microstructure [16]. Kane [17] suggested that most cleaning processes were unique and the best parameter for cleaning were to find the correct balance between the power, wavelength, spot size and traverse speed. The effect on laser cleaning on the hardness, microstructure and surface roughness of the substance was previously reported [18].

Creek [19] suggested that rust reduces the hardness and strength of metals, as the amount of rust reduces, hardness increases. A review of laser cleaning and its effect on the vertical variation over a measured distance (surface roughness) showed that when the average surface roughness increased (more than the wavelength of the laser), absorption increased [20]. For a smooth surface, where average roughness is less than the laser's wavelength, the absorptivity would reduce [20]. Przestacki et al. [21] in the research of cleaning superficially corroded metals by CO_2 lasers found the Ra value to be 1.75µm. Adebayo [22] found in a research on the relationship between graphite flakes sizes and the mechanical properties of grey cast iron that a large, closely-packed flake reduced the strength as well as the hardness. However, Holtzer et al. [23] argued that the presence of a larger flake size increased the ease of machining, good dampening capacity and dimensional stability.

1.3 Research Rationale

The global annual cost of corrosion damage is 2.5 trillion USD [24] . This value was approximately 3.4% of the world's GDP. Around 15-35% (375-875 billion USD) of that cost could be saved globally if corrosion prevention was implemented [25]. In 2002, the United States Federal Highway Administrator (FHWA) released a two-years research on the direct cost of metallic corrosion in nearly every U.S industrial sector [26]. These affected sectors include: manufacturing; production; infrastructures; transportation; aerospace; automobile and many more [26]. Koch *et.al* [26] reported *via* a study on corrosion cost and preventive strategies reported that the annual direct cost of corrosion was estimated at a staggering 276 billion USD which is 3.1% of the nation's gross domestic product. The production and manufacturing sector accounted for 17.6 billion USD which is quite large. The transportation sector accounts for 21.5% (29.7 billlion USD) of the total cost [26] . From these case studies, there are key reasons that justify the need for this research. In particular, laser rust removal helps to decrease the cost of replacing and maintaining metallic engineering parts [27, 28]. The life-span of metallic engineering components can be greatly increased using laser rust removal technique. It also increases profitability and productivity in manufacturing industries by saving production and maintenance time and prevents sudden failure of parts. Controlling corrosion and rusting also ensures the mechanical and physical properties such as hardness, surface roughness, the microstructure is retained even over its life-span post laser cleaning. Furthermore, since rusting occurs naturally, it helps to reduce and control its effect to the barest minimum. Laser-based industrial processes exist for removal of rust, however, very little work is published and addresses the fundamental effects of laser material interaction post laser cleaning, particularly for automotive brake disc which is a novel application. This work not only aims to address the parameters appropriate to remove rust/corrosion from an automotive grey cast iron component, but also aims to improve the surface integrity of the component for longer functional life, and maintenance costs.

1.4 Mechanism of Rust Removal

The process of removing material from a metallic surface through laser radiation can be achieved through various mechanism [29]. The mechanisms can be grouped into three major groups that are evaporation processes (ablation and selective vaporisation). Impact processes (dry and steam cleaning, spallation, photon pressure, evaporative pressure and spallation) and vibration processes (angular laser cleaning and transient thermal heating) can also act as a remedy for cleaning surfaces [30]. The mechanism of laser rust removal using CO_2 laser

applied was based on stimulated emission phenomenon, heating, absorption, melting, and vaporisation. The rust deposition was a thin loose transition layer which was removed with the laser irradiation. This layer is mainly made of Fe_2O_3 and Fe_3O_4 particles [16], as the rusted surface is exposed to high laser power, a laser-absorptive field is naturally formed. This was achieved by the breaking down and ionization of the plasma above the surface. At the same time, the output temperature is above the melting point of the rust particles [18]. The laser energy absorbed is transformed into air or plasma intrinsic energy [16] as shown in Figure 1. In relation to the temperature, the surface absorbed laser power leading to enthalpy (equal to the internal energy of the system plus the product of pressure and volume). The corroded surface is removed since the surface temperature is greater than the vaporisation temperature of the material [31]. Besides the conventional laser cleaning mechanism, other laser cleaning mechanisms are; shot blasting, blast cleaning and shock laser cleaning [32 - 34]. A schematic and expanded representation of rust removal using a laser is shown in Figure 1.

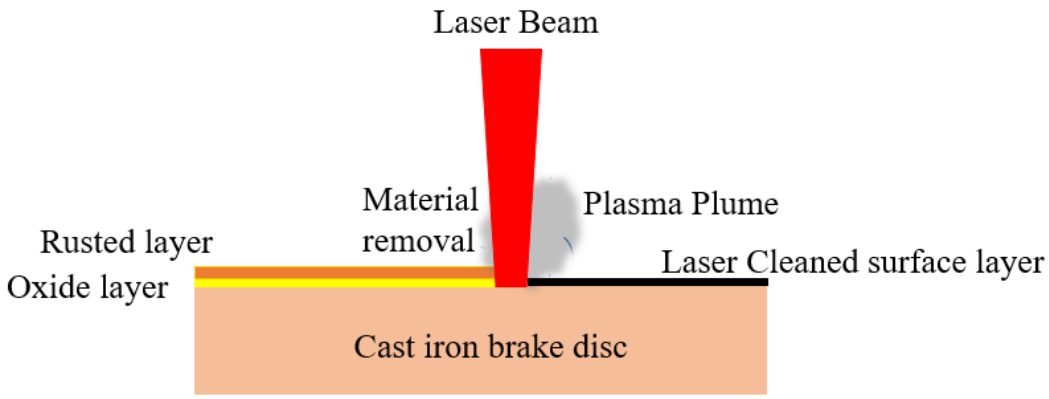

FIGURE 1 A SCHEMATIC REPRESENTATION OF LASER RUST REMOVAL PROCESS.

2 EXPERIMENTAL AND ANALYTICAL TECHNIQUES

2.1 Background of Test Material

The material used for the experiment was both rusted and un-rusted grey cast iron automotive brake disc of a Vauxhall Astra diesel car. The samples were cut from the brake disc into small blocks for ease of laser surface treatment (see Figure 2(b)). The grey cast iron brake disc composes of 3.25 – 3.5 wt% carbon, 0.050 – 0.45 wt% chromium, 0.15 – 0.40 wt% copper, 91.9 – 94.2 wt%, iron, 0.50 – 0.90 wt% manganese, 0.05 – 0.10 wt% molybdenum, 0.050 – 0.20 wt%, nickel, <= 0.12 wt% phosphorus, 1.8 – 2.3 wt% silicon and <= 0.15 wt%

Sulphur [35]. The availability of grey cast iron in abundance makes it the second cheapest of all engineering metals [36]. Due to the operating conditions of the brake disc, it is required to have a good compressive strength, high friction coefficient, considerable lightweight, good thermal capacity and economically viable [37]. The ease of manufacture, cost, anti-wear resistance properties and thermal stability make grey cast iron suitable for the brake disc [38]. The microstructural content contains flaked graphite in a matrix of pearlite and some traces of ferrite [23]. The manufacturing process of the brake disc includes casting, cutting, and forming [39]. It undergoes some heat treatment to change its microstructure thereby boosting its mechanical properties [38, 39].

2.2 Preparation of Sample Prior to Laser Cleaning

Pre-laser treatment involves the preparation of samples prior to laser beam exposure. The brake disc was in its as-received state (un-rusted) at the onset of the experiment. The basic steps involved in the pre-laser treatment involved induced rusting and cutting. These steps are necessary only for the sake of this experiment. The brake disc was exposed to the atmosphere to enable moisture (water and air) to act on it. By the fifth day, uniform rust was formed throughout the entire surface of the brake disc as seen in Figure 2. The uniformly rusted brake disc was then cut into 20 parts (samples) of equal size to ensure that samples were sufficient for the experiment. Figure 2 shows the rusted brake disc and the cut sample into smaller parts prior to laser treatment.

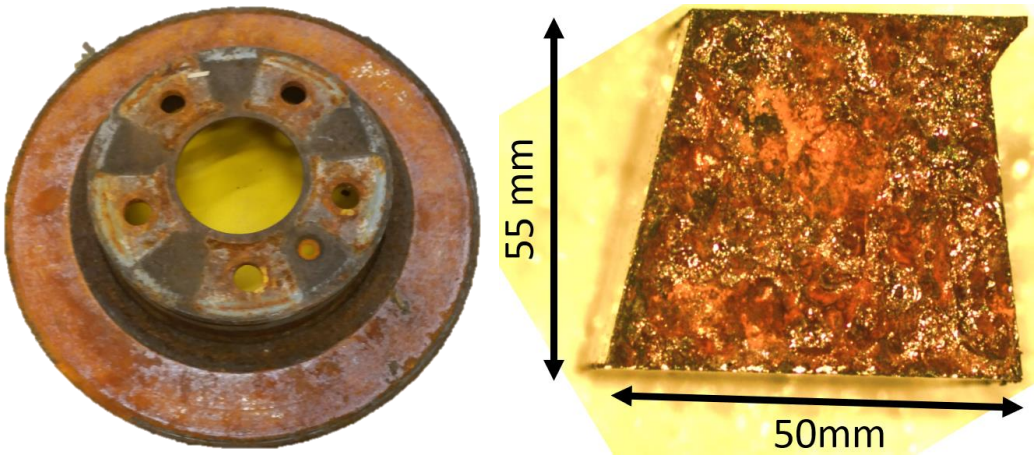

(A) (B)

(C)

FIGURE 2 ILLUSTRATES OPTICAL IMAGES OF THE RUSTED BRAKE DISC IN (A); A CUT BAKE DISC INTO SMALLER PARTS IN (B) AND (C) THE UN-RUSTED AUTOMOTIVE BRAKE DISC.

2.3 Laser Cleaning Process

Laser cleaning experiments were conducted using a short pulse, CW, Rofin multiscan CO_2 laser (Hamburg, Germany). The laser has a wavelength of 10.6µm and a maximum power output of 85W. Experimental parameters applied were, namely: laser power, traverse speed, and spot size and were varied (see Table 1). The plasma generated was channelled out from the laser to prevent it from settling on the galvo-head. A systematic approach was adopted for the experiments where one parameter was changed in an orderly pattern while other parameters were kept constant. The experiment involved 20 different samples with a total of 27 trials each processed with a unique set of processing parameter. First, the power was varied between 10W to 85W (maximum power) while other parameters were kept constant. The Radiance density (brightness) was determined using our previous technique [40 – 42], and ranged from 2.74 - 132.35 $W.mm^2.Sr^{-1}.\mu m^{-1}$. Traverse speed was varied between 30 to 3000mm/s with other parameters being kept constant. The focal distance was also varied to obtain the correct laser beam diameter. Each of the cut samples was mounted on the processing table and exposed to the CO_2 Laser beam to remove the top rust surface (see Figure 3(a)). Figure 3 also shows the experimental set up during the laser cleaning process and the method of rust removal.

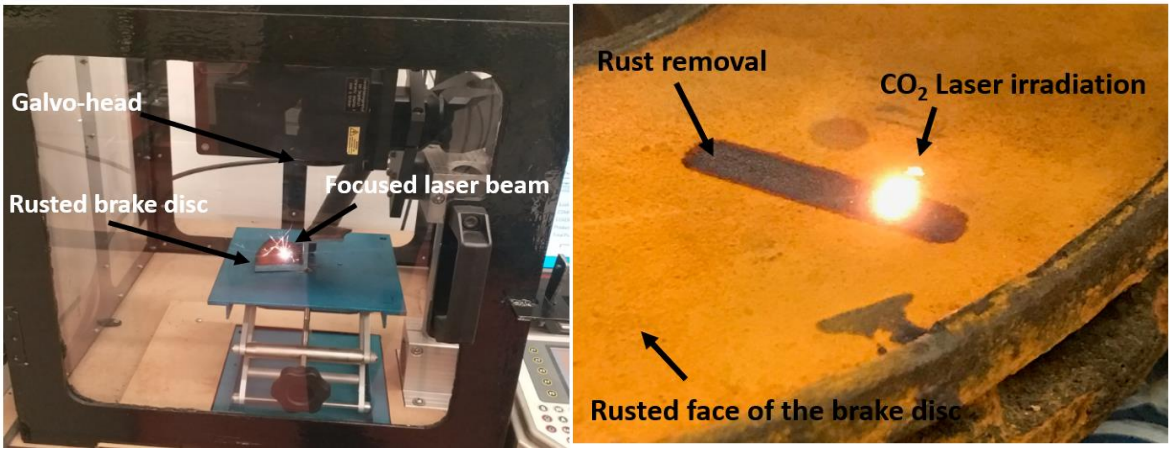

(A) (B)

FIGURE 3 SHOWING EXPERIMENTAL SET-UP OF THE CO_2 LASER RUST REMOVAL PROCESS IN (A) AND METHOD OF RUST REMOVAL IN (B).

TABLE 1 LASER PROCESSING PARAMETERS EMPLOYED FOR LASER RUST REMOVAL

Power (W)	Traverse speed (mm/sec)	Beam diameter (mm)	Radiance Density ($W.mm^2.Sr^{-1}.\mu m^{-1}$)
10 -85	30 - 3000	0.71 - 1.69	2.74 - 132.35

2.4 Material Removal Measurement

The micrometre screw gauge was used to measure the thickness of the samples before and after laser rust removal. The as-received thickness of the sample was also measured, and the difference in thickness was noted. The process was used to determine the ablation depth as well as measure the amount of material removal post laser cleaning. Measurements were taken five times on every sample to ensure a level of accuracy, and the average was then calculated.

2.5 Micro-Hardness Testing, Topography, Sample Preparation and Etching Procedures

The Mitutoyo MvK-H1 hardness tester (Kawasaki, Japan) was used to measure the Vickers micro-hardness. A maximum load of 1000N was applied on the samples with a 5 secs dwell time. A Bruker contour GT profilometer with the vison64 software was used to measure the surface profile of the samples with the aim of quantifying the roughness. Polished cast iron specimen usually shows little or no matrix microstructure. Etching was conducted on the un-

rusted as well as totally rusted and the best laser-cleaned samples. The etchant used for the etching of the grey cast iron samples was Nital. Prior to etching, the samples were cut down from the whole automotive brake disc to smaller pieces. Samples were cross-sectioned for microstructural analysis. Selected samples were and mounted using a standard cold mounting Vari-set 20 cold mounting powder and the quick-set cold mounting liquid. The mixing ratio was 2-parts powder to 1-part liquid by volume. The samples were kept at the center of the mount with the surface to be polished facing downward. The polishing process was conducted in 6 phases. A 9µm DiaDuo-2 water-based diamond suspension containing monocrystalline diamonds was used as the cooling lubricant and polish liquid. A MD-Dur cloth was used, and the process took place at a speed of 150rpm for 10mins. A 6µm DiaDuo-2 diamond suspension with a MD-Dur cloth at a speed of 150rpm for 7mins. A 3µm DiaDuo-2 paste diamond suspension polish liquid was used with a MD-Dac cloth at 150rpm for another 7mins. A 1µm DiaDuo-2 paste diamond suspension polish liquid was used with a MD-Dac cloth at 150rpm for 3mins. Final polishing was then carried out using the colloidal silica suspension (0P-S) as the cooling lubricant for 3mins at 150rpm. To obtain a top-notch polish surface, the sample was then transferred to the Buehler Vibromet 2 vibratory polisher for 2 hours.

2.6 Optimisation of properties using Gaussian Process Regression

A Gaussian process regression (GPR) approach [43] was used to predict the effects of laser cleaning with respect to the process parameters based on the experimental data. GPR is a reliable and a well-known method in machine learning that can be deployed using various types of data. It is a non-parametric approach and has been used widely to solve a variety of problems such as material properties, thus, can be deployed to understand the effects herein in relation to laser processing related issues.

3 RESULTS AND DISCUSSION

3.1 Selection of Laser Cleaning Parameters

Figure 4 represents a rusted surface which was then was removed by varying the laser parameters. The rusted surface comprises heavily corroded regions, corrosion cracking, and some areas that are partially rusted. When the laser altered from 10W to a max of 85W, it was observed that a very low level of rust was removed and no visible effect of rust removal was evident at 10W. As the laser power was ramped up to 20W, the effect of rust removal became visible, but surface still contained significant rust. Upon applying 30W to 40W of laser

power, there was a moderate level of rust removal. As the laser power was increased to 50W, there was a considerable amount of rust removed. At 60W, the rust removal was increased but still contained areas where rust was visible. Although, it offered the best effect as ramping up the laser power to 70W removed, the rust significantly, but also affected the base metal. Thereafter, the rust was removed but the base metal was considerably altered due the increased laser power applied, and the substrate becomes visible with melt zones evident in Figure 5(a), (b) and (c).

As mentioned, increasing the laser power to 60W resulted to the best laser cleaned surface and will be further applied (Figure 5(e) and (f)) whilst varying the traverse speed. The best laser cleaned sample after varying all the parameters was 60W, 900mm/s traverse speed and 0.72mm spot size as all the rust were removed and the metal substrate was not melted (see Figure 5 (e) and (f)). Figure 4 demonstrates a direct comparison between the rusted (untreated) sample and the laser cleaned surfaces in Figure 5 (a) to (f).

Laser power (60W) and a spot size of 0.72mm was kept constant while the traverse speed was varied, from 30mm/sec to 100 mm/sec, all rust was removed, and base metal was badly affected due to very low mark speed which was due to the high laser power acting on the cast iron for a prolonged period which caused considerable melting. This would not be desirable as it is then likely that some of the surface properties would have changed. For the application of a brake disc; modification in the materials surface integrity was not an objective since it will affect the functional capabilities of the brake disc. Rust was removed from the base metal as it was moderately affected when traverse speed was increased to 200mm/sec to 300mm/sec. Likewise, the rust removal was affected in the same manner with slightly higher removal from 500mm/sec to 700mm/sec. At 900mm/sec, there was excellent removal of rust, and base metal was not affected which is rather desirable. At 1000 mm/sec, a good level of rust removal with little rust particles still seen on the surface. Beyond this speed (1500, 2000, 3000 mm/sec) rust was not removed to any considerable effect as the traverse speed was too fast to create any heating, local melting and material removal.

The spot size was varied from the largest diameter (1.69mm) obtainable based on the focal height of the galvo head of the laser to a smallest of 0.71mm. It was concluded that to obtain the best effects and fully remove the rust layer off the grey cast iron brake disc; a minimal spot diameter was rather effective and desirable (0.71mm). Larger spot diameter at maximum

laser power left many rusted regions. Thus, the best surface condition was obtained using a fairly small spot diameter focused into the material and was 0.72mm.

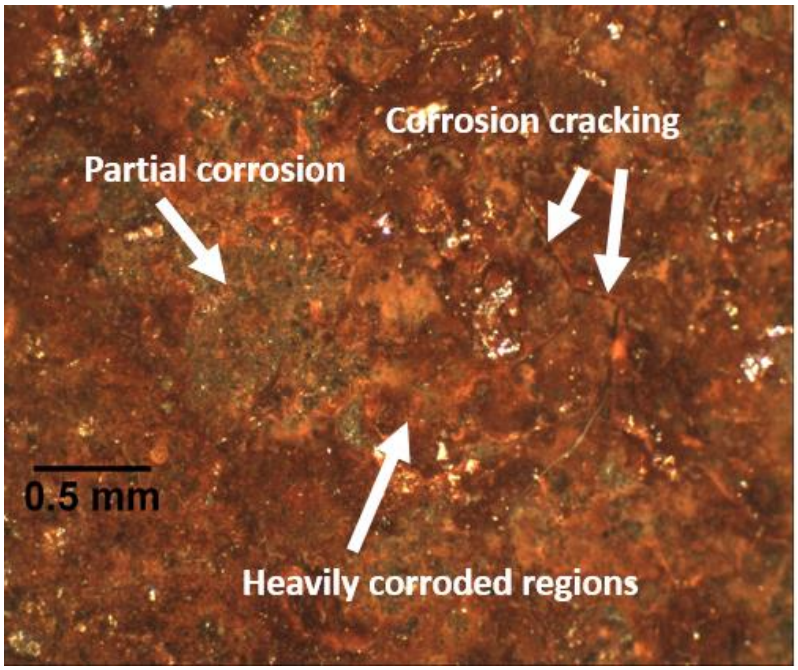

FIGURE 4 OPTICAL IMAGES OF THE RUSTED (UNTREATED) SURFACE.

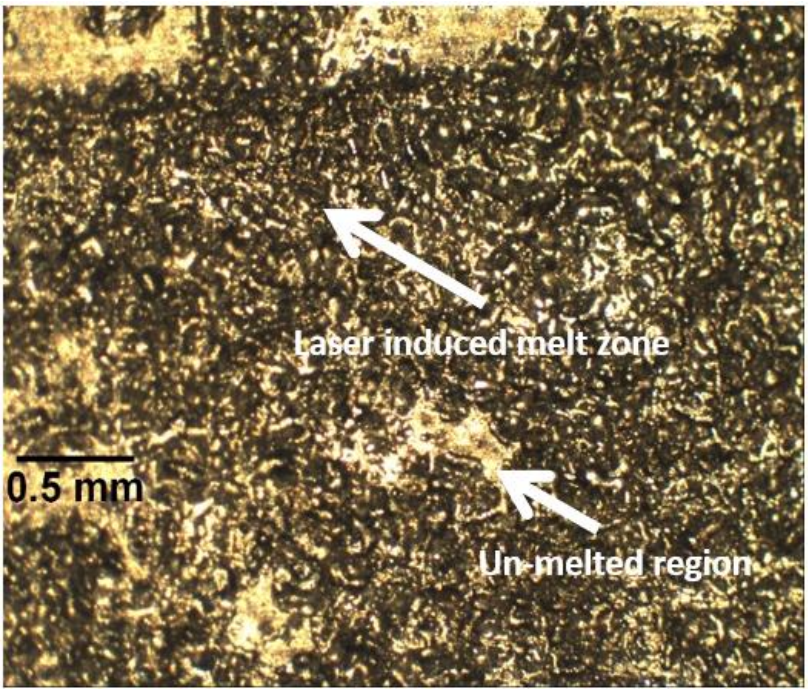

(A)

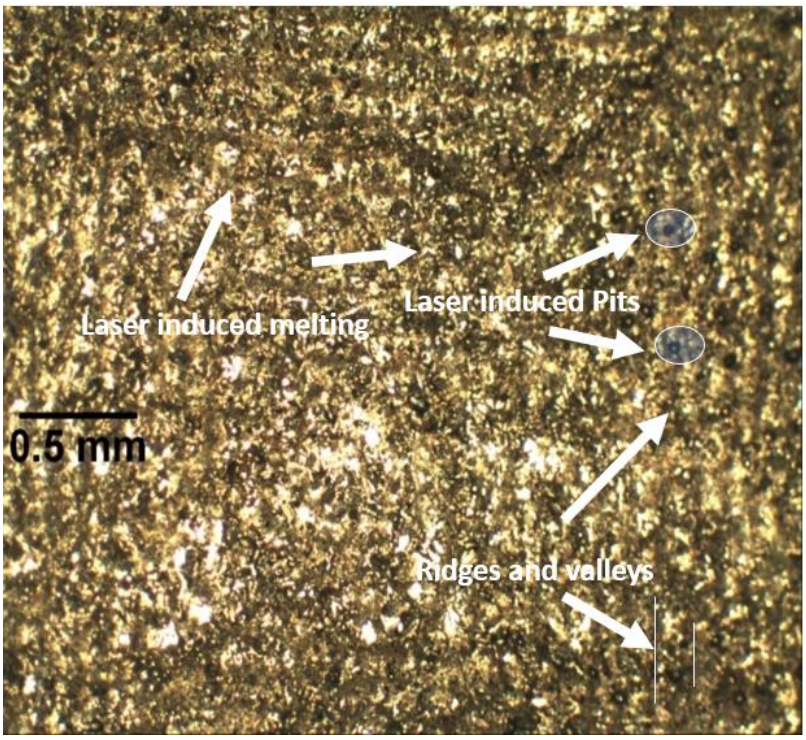
Laser induced melting
Laser induced Pits
0.5 mm
Ridges and valleys

(B)

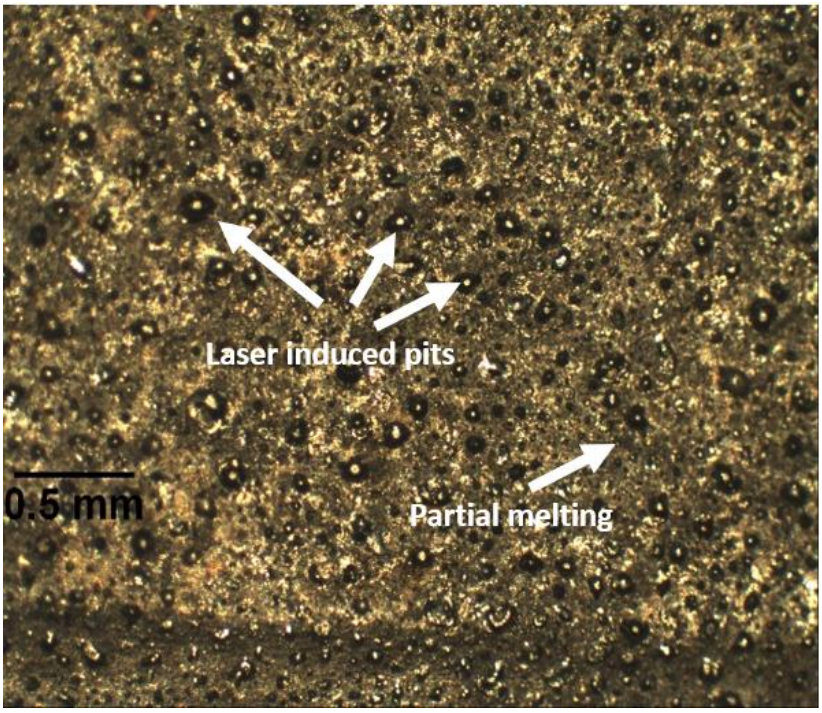
Laser Induced pits
0.5 mm
Partial melting

(C)

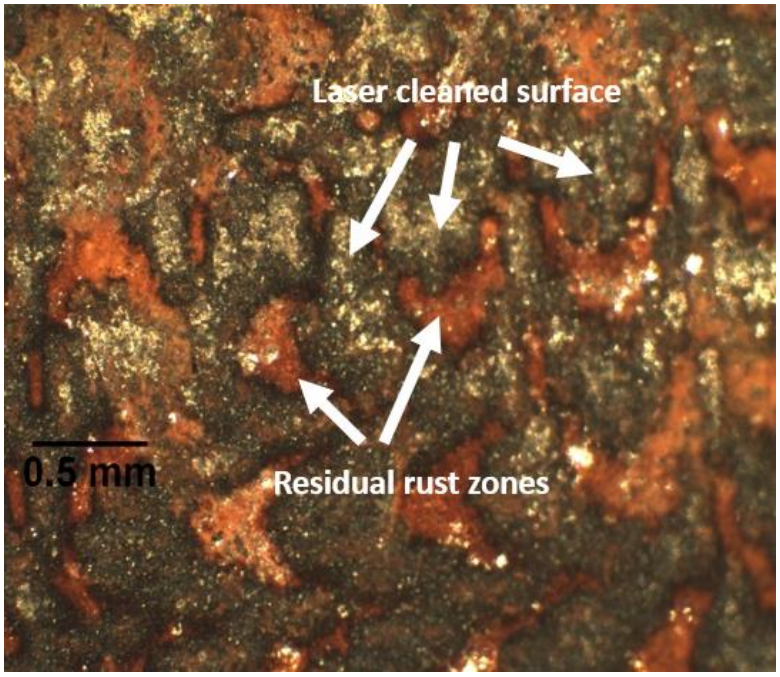
Laser cleaned surface
0.5 mm
Residual rust zones

(D)

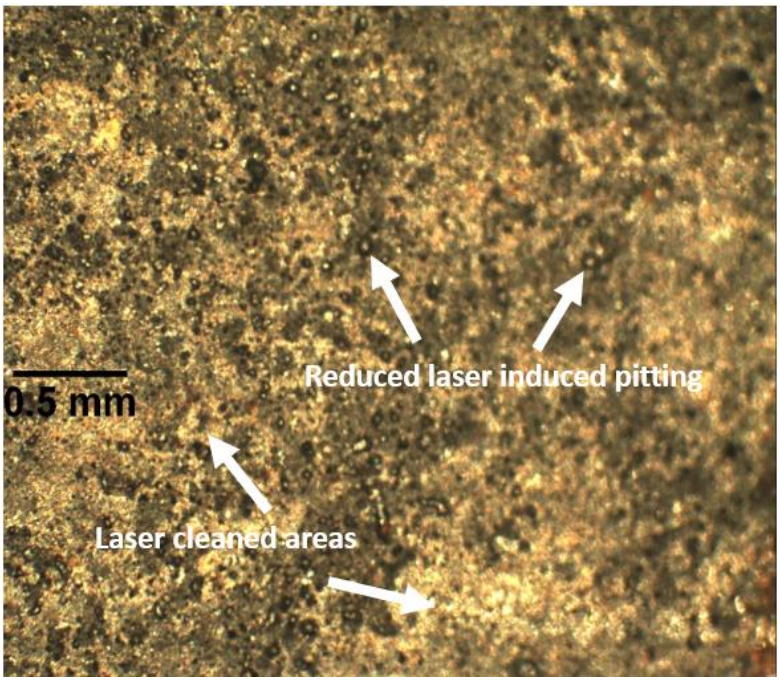
Reduced laser induced pitting
0.5 mm
Laser cleaned areas

(E)

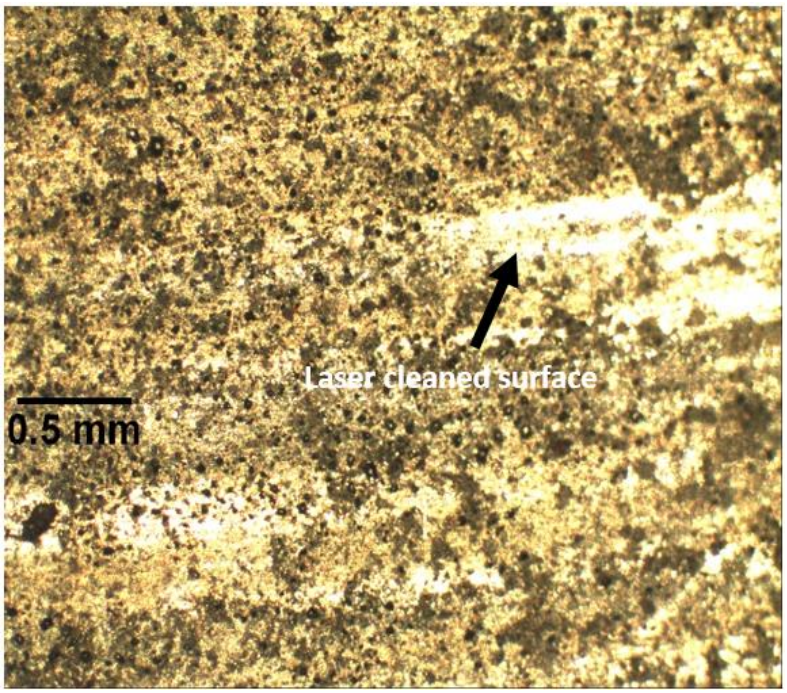

(F)

FIGURE 5 OPTICAL IMAGES OF LASER CLEANED SURFACES IN (A) AT 30MM/SEC; AT 300MM/SEC IN (B); AT 600MM/SEC IN (C); AT 2000MM/SEC IN (D) WHILST USING A SPOT DIAMETER OF 0.72MM AND LASER POWER OF 60W. (E) AND (F) SHOWING THE MOST APPROPRIATE LASER CLEANED SURFACES WITH A SPOT DIAMETER OF 0.72MM AND LASER POWER OF 60W AT 9000MM/SEC.

3.2 Measurement of Rust Removal

Mathematically, the depth of ablation ($Z_{ablation}$) is determined by the difference between average rusted sample thickness, and the average laser cleaned sample thickness is given by Equation (1):

$Z_{ablation}$ (mm) = average thickness of rusted sample – the average thickness of laser cleaned sample……..…….. (1)

Using the un-rusted surface as a reference, the deviation can serve as a characteristic to denote how much rust was removed from each sample. Deviation from the un-rusted sample can be represented as:

Deviation (mm) = average thickness of laser cleaned sample – the average thickness of as-received...…….(2)

The rusted brake disc has a slightly varying thickness of corrosion as it was exposed to the atmosphere. However, several measurements were taken at various points on each sample and the average was calculated. Hence, the mean represents the most accurate thickness value. Table 2 shows the average thickness of the surfaces with three different conditions. It was observed that the average thickness of the rusted layer was 0.33mm compared to the un-rusted surface. The thickness of the laser treated surfaces is shown in Table 2 as well as the depth of the rusted layer removed in Table 4. During the experiment, the cast iron brake discs were subject to high local temperatures generated from the laser beam operation at high power and or low traverse speed. Hence, it becomes unnecessary to measure the amount of rust removed after the top surface was melted and solidified, leading to the formation of melt zone, and pits, and dimples, as evident in some of the optical images in Figure 5(b) and (c).

The GPR curve determined using the experimental data (laser power *versus* Z-ablation) combined with the optimized fit is shown in Figure 6. It was clear that the increase in laser power had increased the Z-ablation which peaked at 60W with 0.30mm in thickness of rust removed. It then began to decline. The value of Z-ablation began to reduce beyond this point and can be postulated (from Figure 6) to saturate where the ablation depth would then maintain with laser power increases up to 200W. The dip in the curve is difficult to explain at this stage, but it can be given to the lack of experimental data which reduces the reliability of the GPR method. Reliability would improve with further experimentation which would verify and support the predicted GPR curve.

TABLE 2 THICKNESS OF BOTH THE UN-RUSTED AND RUSTED SURFACE.

Sample Type	Reading 1 (mm)	Reading 2 (mm)	Reading 3 (mm)	Average(mm)
Un-rusted	8.18	8.22	8.20	8.20
Rusted	8.52	8.57	8.49	8.53

TABLE 3 THICKNESS OF RUST REMOVED AND ABLATION DEPTH

Laser Cleaning Parameters (Power, Speed, Spot Size)	Average thickness (mm)	$Z_{ablation}$ (mm)	Deviation (mm)
10W, 1000 mm/s, 0.72 mm	8.49	0.04	0.29
20W, 1000mm/s, 0.72mm	8.46	0.07	0.26
30W, 1000mm/s, 0.72mm	8.37	0.16	0.17
40W, 1000mm/s, 0.72mm	8.31	0.22	0.11
50W, 1000mm/s, 0.72mm	8.27	0.26	0.07
60W, 1000mm/s, 0.72mm	8.23	0.30	0.03
60W, 900mm/s, 0.72mm	8.25	0.28	0.05
60W, 1000mm/s, 0.72mm	8.31	0.22	0.11
60W, 1500mm/s, 0.72mm	8.39	0.14	0.19
60W, 2000mm/s, 0.72mm	8.45	0.08	0.25
60W, 3000mm/s, 0.72mm	8.49	0.04	0.29
60W, 900mm/sec, 0.72mm	8.21	0.32	0.01
20W, 1000mm/s, 0.72mm	8.24	0.29	0.04

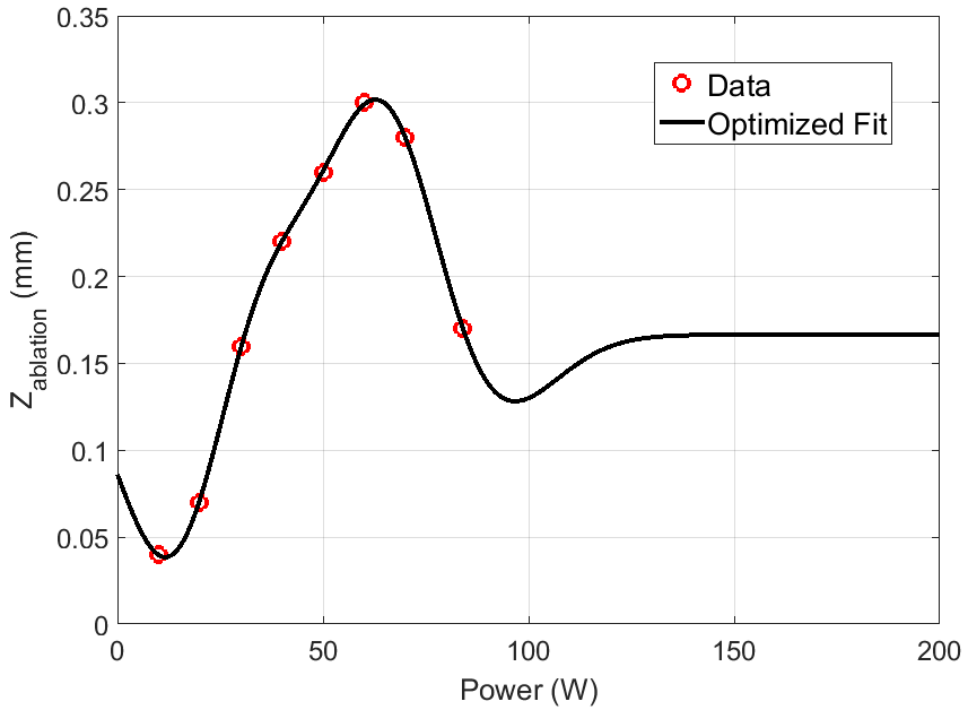

FIGURE 6 EXPERIMENTAL DATA WITH OPTIMIZED FIT FOR LASER POWER *VERSUS* Z-ABLATION OBTAINED WITH THE GPR METHOD.

3.3 Micro-Hardness Analysis

Table 4 presents the variation in hardness measured for the cast iron brake disc at various surface conditions applied. The average hardness of the un-rusted surface was measured to be 224 HV. This was verified by the previous work on the manufacturing of grey cast iron automotive brake disc that reported a Vickers hardness value of 225 HV [44]. On the other hand, the hardness of the rusted surface was the lowest at an average of 93HV. This was natural since the rust particles formed on the brake disc were loosely packed and the bond strength of these particles was not as strong as that of the un-rusted surfaces to render the hardness to be high comparatively. Table 5 presents the hardness values with respect to the rust layer thickness. It was evident that the thicker the rusted layer, the lower the hardness which is due to the penetration depth of laser light, which diminishes as the depth of rust increases. When these surfaces were compared to those cleaned with a laser; there was a trend of increased hardness with the lowest laser cleaning traverse speed. The lowest traverse speed comprised of the highest hardness – an increase by 37% in comparison to the un-rusted surface and over 3 folds increase compared to the fully rusted surface. Creek [19] suggested that rust reduces the hardness and strength of metals, as the amount of rust reduces, hardness increases. Further, when as the traverse speed increased the hardness decreased. At 900mm/sec, the hardness was measured at an average of 235HV which was about 4.5% in comparison to the un-rusted surface. The traverse speed was increased to 1500mm/sec and the hardness was measured to be 178 HV. This was the lowest obtained from the laser cleaned surfaces. This was attributed to the fact that higher traverse speed did not result in enough rust being removed from the respective surface which leads to the hardness still not measuring close to the un-rusted surfaces. Tabulating these parameters into the GRP curve also yielded similar findings, whereby, the hardness reduced as the traverse speed increased (see Figure 7). As the laser beam was active for a longer time period on the rusted surfaces. Particularly at low traverse speed (30mm/sec), there was significant heat being generated at the laser-material interaction. Thus, the possibility of removing the rust was not only high as evident from Figures 5, but also producing partial melt-zones which solidified at a slower rate to have generated a ductile surface. Also, the surface partial-solidification induced ductile nature would be able to sustain for plastic deformation during cyclic fatigue failure of the specimen.

TABLE 4 SHOWS THE MICROHARDNESS OF VARIOUS SURFACES.

Sample Condition	Hardness (HV)					
	Trial 1	Trial 2	Trial 3	Trial 4	Trial 5	Average
Un-rusted	224	224	224	223	224	224
Rusted	91	94	90	97.0	95	93
60W, 900mm/sec, 0.72mm	234	238	233	235	236	235
60W, 1500mm/s, 0.72mm	176	175	180	175	182	178
60W, 30mm/s, 0.72mm	307	310	302	305	305	306

TABLE 5 VICKERS MICROHARDNESS VALUES WITH RESPECT TO RUST THICKNESS.

Surface Condition	Micro-hardness (Hv)	Rusted Layer Thickness (µm)
Rusted surface	93	330
Partially rusted surface	178	190
Un-rusted surface	224	10
Best laser cleaned surface	235	0

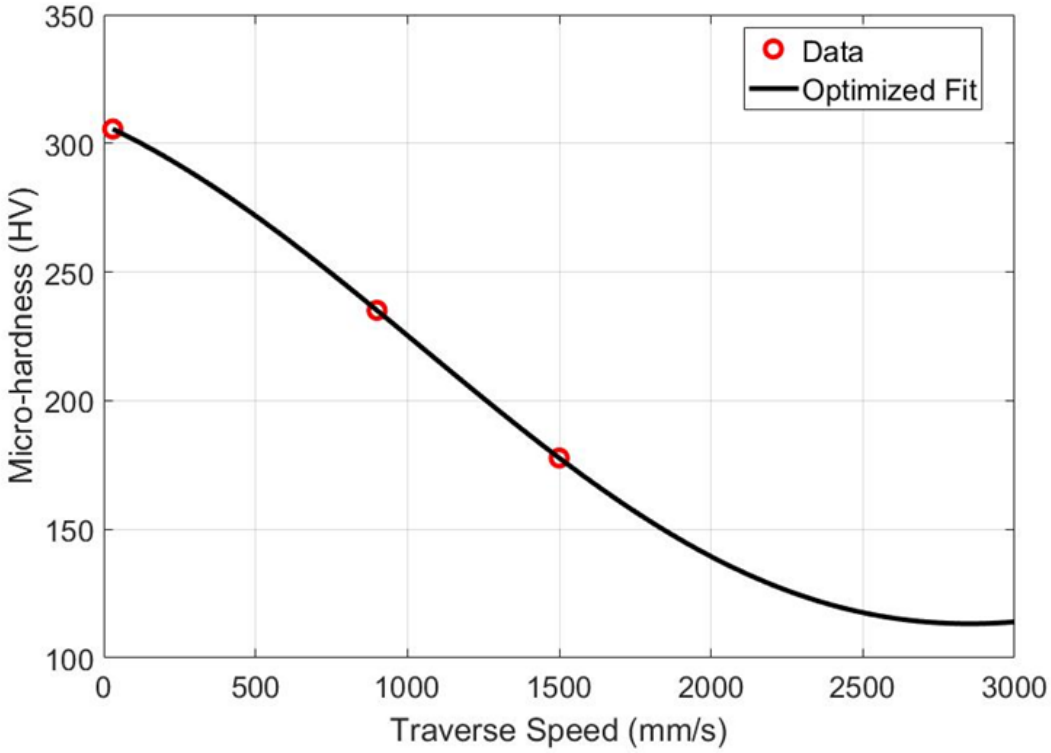

FIGURE 7 GPR OPTIMIZED CURVE AND EXPERIMENTAL DATA OF MICROHARDNESS *VERSUS* TRAVERSE SPEED.

3.4 Surface Roughness Analysis

The average roughness (Ra) is a 2-D roughness parameter showing the arithmetic average of the absolute values of the profile heights with respect to the mean over a given length. In this case, it was significantly high for the rusted cast iron brake disc with a measured value of 55.41µm. When this was compared to the un-rusted brake disc, the measured roughness was 3.08µm and was considerably lower. This was due to the onset of some rust particles formed and the exposure to the environment and operating conditions that ultimately lead to heavy rust formation at a later stage. However, after laser cleaning - the surface became much smoother. The roughness was measured to be 1.29 µm and was less than 50% compared to the un-rusted brake disc. As expected, the Rt value for the three surfaces shown in Table 6 had a similar trend with the rusted surface having a value of 230.39µm. The best laser-cleaned and un-rusted surface had an Rt value of 26.27µm and 24.89µm respectively. It was observed that even though the best laser-cleaned surfaces had a smaller Ra value when compared to the un-rusted sample, which however comprised of a higher Rt value. This indicated the onset of the Gaussian laser beam ablating the surface of the cast iron brake disc. This in turn, lead to increasing the distance between the lowest and highest points over the surface area of the laser-cleaned samples than that of the un-rusted surface. The 2-D

topographical images of the rusted, un-rusted and totally cleaned samples are illustrated in Figure 8 to Figure 10 respectively. From Figure 8 to Figure 10, it is was seen that the rusted sample 2-D topography has a less smooth surface when compared to the other two samples. The existence of pits, ridges and valleys might have influenced such topography.

Upon observing the Sa values, it was evident that as the laser power increased, the Sa values also began to increase and peaked at 30W, then reduced as the laser power went up (see Figure 11). This indicated that the surface was smoothening as the roughness was reduced with the rusted layer being removed. At 60W the roughness was at the lowest with a possibility of complete removal of the rust. The roughness then began to increase as the as the laser power went up. This indicated that there was a possibility of surface melting and reforming to form a new topography which created a rougher topography. This was also evident from the optical images showing melt zone beyond the laser power of 60W. As the surface considerably melted, it created dimpling and pitting effects, evident in Figure 12. This created an increase in the surface roughness which increased the Sa values as evident from Figure 12 that the roughness began to improve.

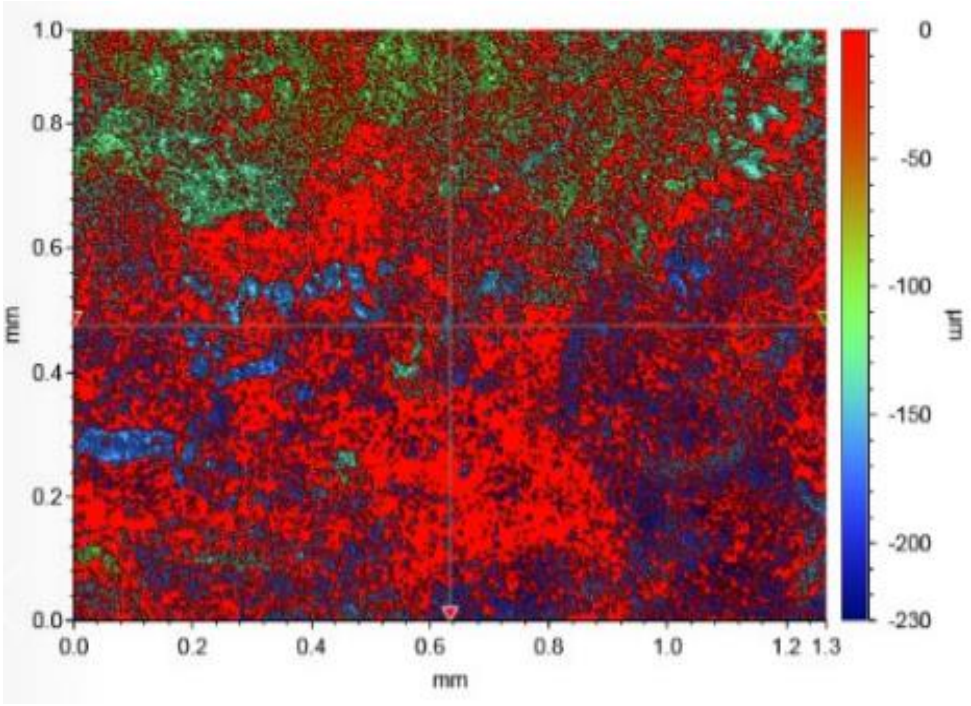

FIGURE 8 TOPOGRAPHY OF RUSTED GREY CAST IRON BRAKE DISC SURFACE.

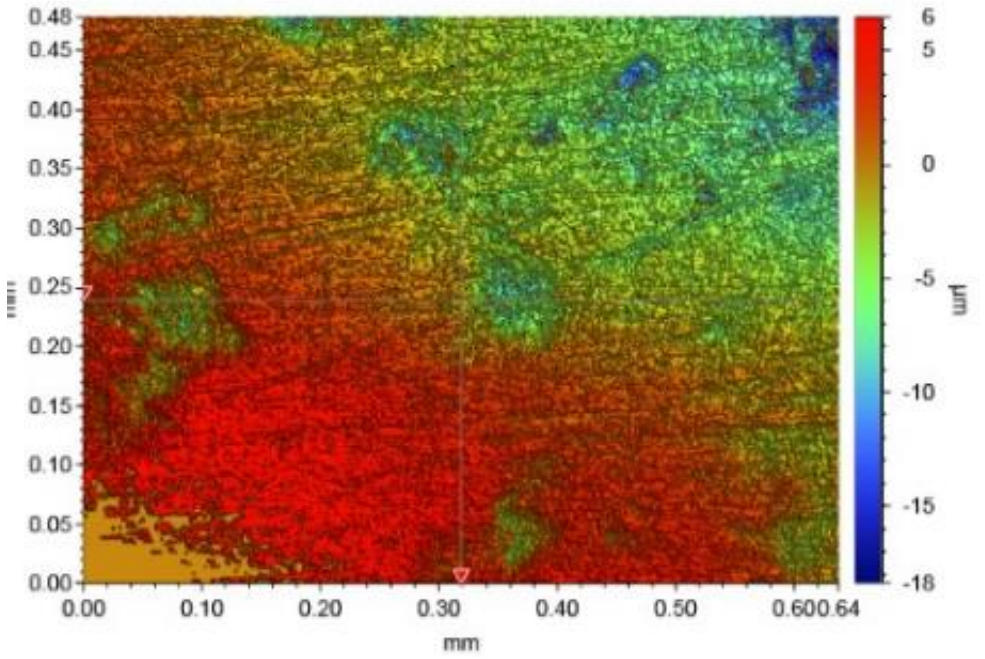

FIGURE 9 TOPOGRAPHY OF UN-RUSTED GREY CAST IRON BRAKE DISC SURFACE.

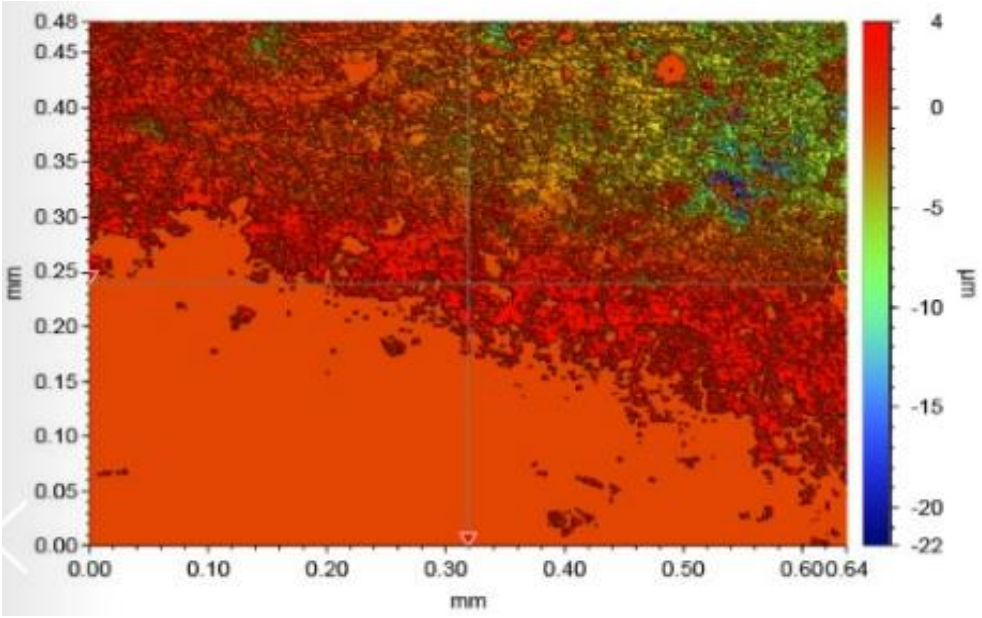

FIGURE 10 TOPOGRAPHY OF LASER CLEANED GREY CAST IRON BRAKE DISC AT 60W LASER POWER, 900MM/SEC AND 0.72MM SPOT SIZE.

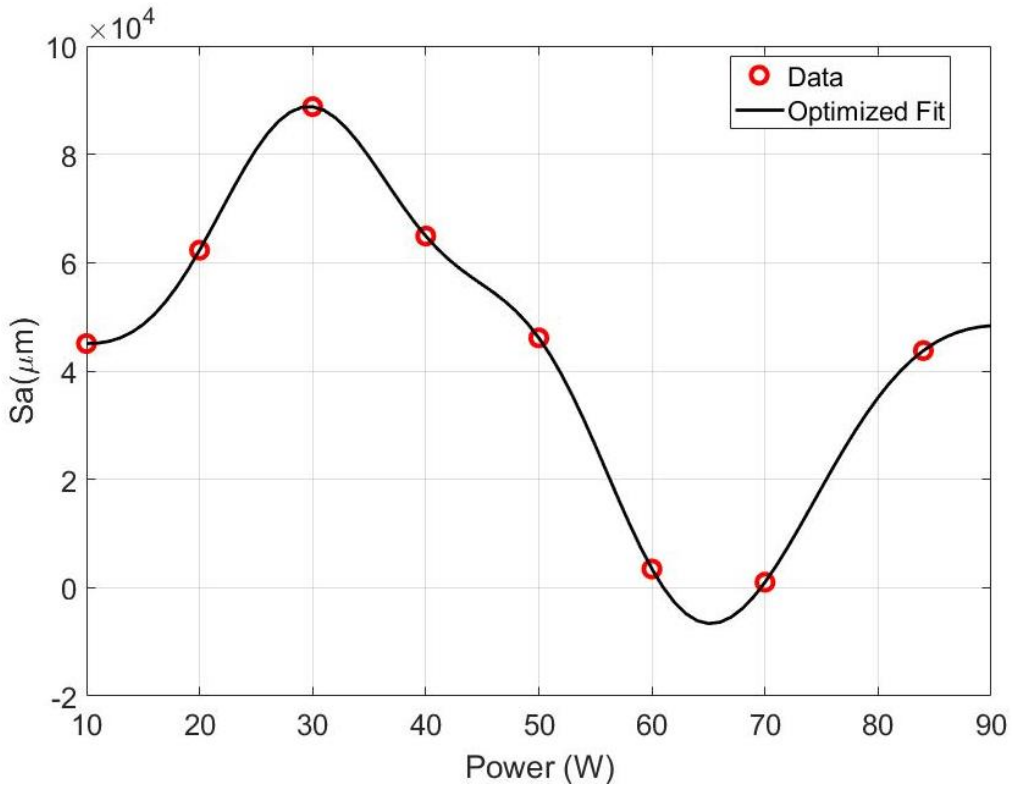

FIGURE 11 ILLUSTRATING THE Sa VALUES WITH RESPECT TO INCREASE IN POWER (60W LASER POWER, 900MM/SEC TRAVERSE SPEED AND A SPOT SIZE OF 0.72MM).

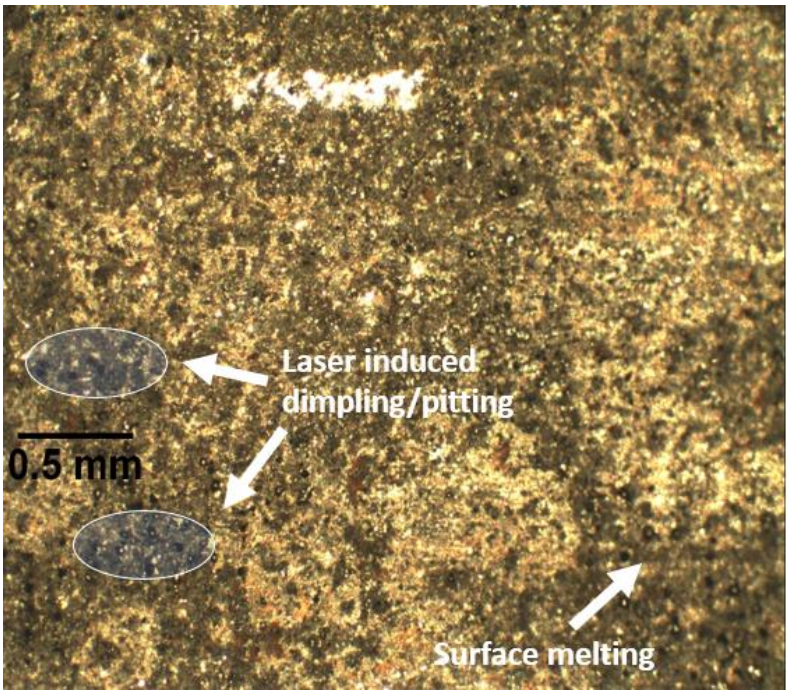

FIGURE 12 SHOWING THE ROUGHENING OF THE SURFACE AT 70W LASER POWER, 900MM/SEC AND 0.72MM SPOT SIZE AS MELT ZONES BEGIN TO TAKE PLACE IN VARIOUS AREA.

3.5 Microstructural Analysis

The microscopic images of the un-rusted, rusted and best laser-cleaned surface are shown in Figure 14 to Figure 16. The microstructural images of the three surfaces all show the presence of a black flake-like structure (graphite flakes). Grey cast iron is characterised for having a large portion of its carbon in the form of graphite flakes. The fast interstitial diffusion of small carbon atoms makes the formation of graphite flakes possible. As diffusion progresses, more graphite is formed. The plane of such graphite is held by a covalent bond and has a hexagonal structure. The presence of silicon as one of the alloying elements of grey cast iron promotes the formation of ferrite and graphite. It acts as a strong graphitizer during eutectic solidification of grey cast iron. Eutectic cells are formed by the nucleation of graphite. The mixture of graphite and austenite makes up the eutectic cells. The eutectic cells can be viewed on the micrograph chemical etching. During the eutectoid transformation, the austenite transforms into ferrite and cementite or graphite. The system stability is dependent on the transformation that occurs. Graphite or cementite either occupies the carbon-rich zone based on the system stability, that is, if the system is metastable, it prefers cementite. If the system is stable, it prefers graphite. The graphite flake is seen to be much softer than the surrounding matrix which is viewed as a void. The formation of the pearlitic matrix with graphite particles occurs in the surrounding matrix of the flake to prevent the structure from being too weak. This formation gives it good compressive strength, good thermal conductivity and vibration damping. It was observed from the microstructure that the graphite flakes vary in shape and size. The rusted sample showed larger flakes than that of the un-rusted and laser-cleaned surfaces. It also exhibits relatively longer graphite flakes on the average. Deep black pits are also seen on the microstructure of the rusted sample which signifies the presence of impurities and non-metallic inclusions. The presence of inclusions and impurities along with the slightly longer and larger graphite flake is responsible for the low hardness value and high Ra value of the rusted sample.

The laser-cleaned sample has a relatively comprised of larger spacing between the flakes when compared to the un-rusted and rusted surfaces. An increase in space between flakes results in an increase in the strength and a corresponding increase in hardness. A relatively shorter flake length and smaller flake size resulted to a higher hardness value when

comparing to the un-rusted and the rusted surfaces. This was because the graphite particles are generally softer. The hardness was evident after laser cleaned surface microstructure in Figure 15 with a decrease in the reduction of graphite flake when compared to the rusted grey cast iron microstructure. Furthermore, a denser cluster of graphite flakes with relatively bigger flake size and longer flake length created lesser space for a hard pearlitic matrix. The grey region in Figure 13 to Figure 15 represents a pearlitic matrix. The pearlitic matrix contained two phases which are ferrite and cementite. While cementite is a hard and brittle intermetallic compound, ferrite has low strength and high ductility. Besides the cementite found in the pearlite matrix, the micrograph also showed no evidence of cementite. The dual phase involving ferrite and cementite which creates the pearlitic matrix originates from the austenite phase. At higher temperature, only austenite is present with 0.76%C would be dissolved in solid solution in the face centred cubic (FCC) crystal. The cooling down of iron to 727°C results in several simultaneous changes. It is highly likely that the laser cleaning process induced temperatures above that level. First, the iron changes from FCC austenite to body-centred cubic ferrite, but the ferrite can only accommodate 0.022% carbon in solid solution. The excess carbon left was then rejected forming the carbon-rich intermetallic phase which is cementite.

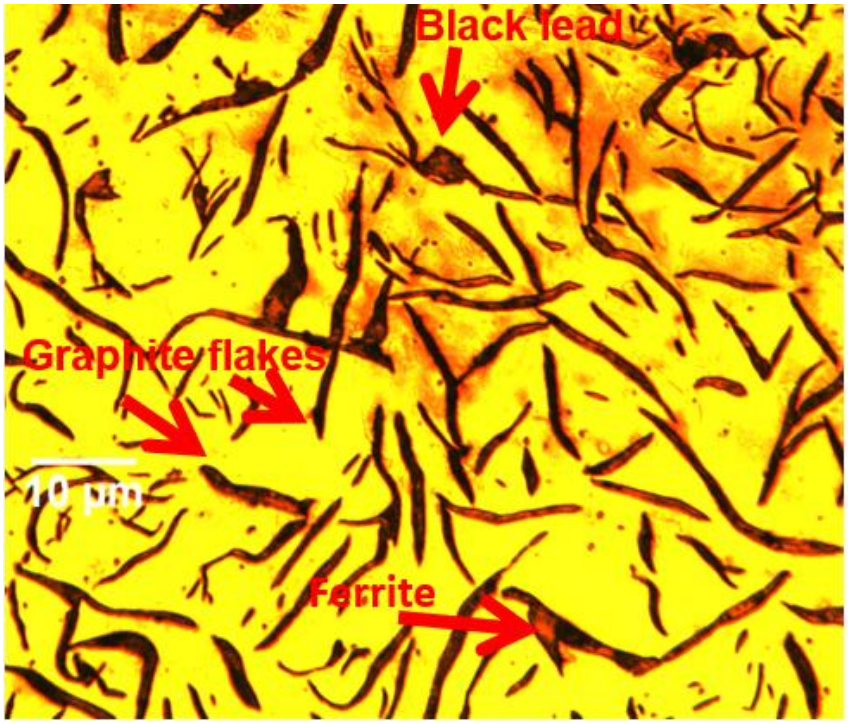

FIGURE 13 MICROSTRUCTURE OF THE UN-RUSTED SURFACE OF THE GREY CAST IRON .

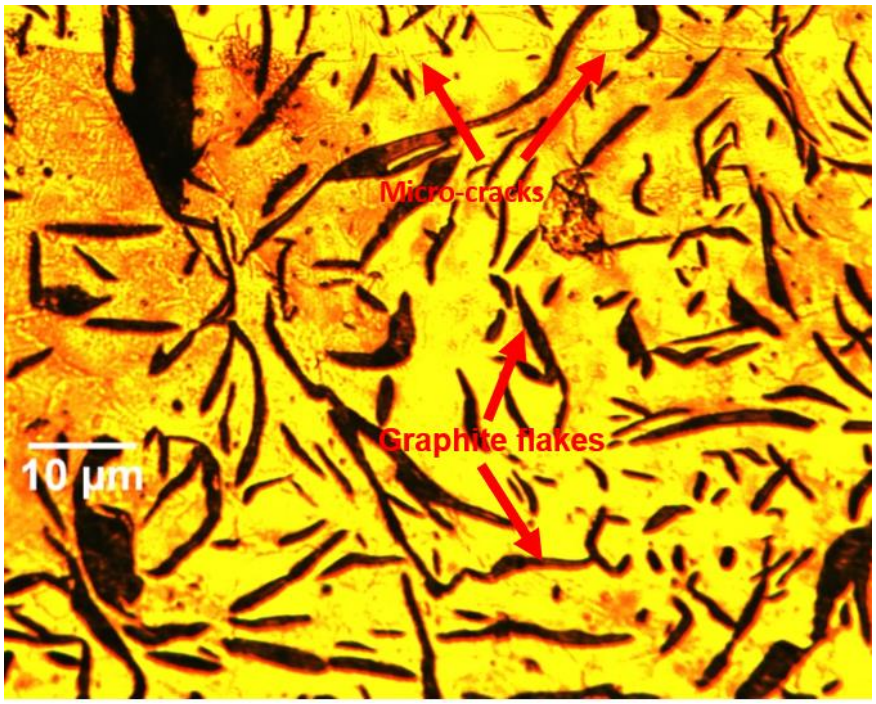

FIGURE 14 MICROSTRUCTURE OF RUSTED SURFACE.

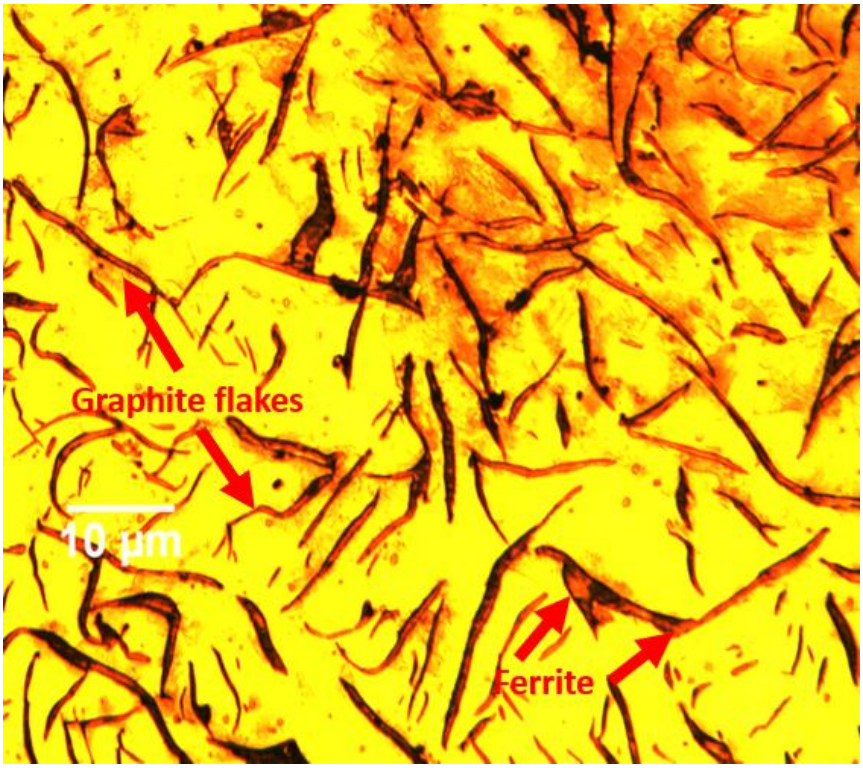

FIGURE 15 MICROSTRUCTURE OF A LASER-CLEANED SURFACE (60W OF LASER POWER, 900MM/S TRAVERSE SPEED, SPOT SIZE OF 722µM).

4. CONCLUSIONS

The enhancement of the surface integrity of a rusted, grey cast iron automotive brake disc was achieved *via* a laser cleaning process. Laser cleaning and rust removal are fast and effective in enhancing the surface integrity of such material. The results showed that the presence of rust on cast iron reduces its mechanical and physical properties. The ripple effect of such reduction leads to failure of the brake disc when fused into the braking system of an automobile. The best set of laser parameter for removing rust from the grey cast iron brake disc using a CO_2 laser system was 60W of laser power, 900mm/s traverse speed and a spot size of 0.72mm. The presence of rust on the surface of the brake disc greatly reduces its microhardness. The laser cleaning process positively altered the microhardness value. There was an increase of 5.04% when comparing the un-rusted sample (223 HV) to the best-cleaned sample (235 HV). The presence of hot spots and brake disc lining on some samples was responsible for some high Ra value. The best-cleaned sample has an Ra value of 1.29µm which is relatively good compared to the un-rusted surface. The microstructural analysis of the samples showed that the presence of randomly distributed graphite flakes surrounded by a pearlitic matrix containing ferrite and cementite. The GPR technique can demonstrate and predict parameters beyond the experimental data. However, further work verifying the prediction will improve its reliability for laser processing problems such as the one herein. The applied parameters showed that laser cleaning could be successfully applied to not only clean rusted surfaces of metallic materials such as the one herein but could also have a positive effect on some of the material properties, thus, increasing the lifetime of the brake disc. Laser cleaning of the brake disc will drastically reduce cost (maintenance and replacement cost). It also prevents sudden failure since the parts have been enhanced to be more durable and reliable, even when operating under harsh conditions. It is also much greener and has the potential to replace chemicals, abrasive materials or shot blasting and harmful cleaning solvent that poses hazards to the end-user.

REFERENCES

1. Hays, G.F. (2012). *Now Is the Time*. World Corrosion Organisation. 1-2, Retried on 25th December 2015, from http://events.nace.org/euro/corrodia/Fall_2010/wco.asp
2. Chare I.A., Jeffery R. and Melchers R.E. Rust removal from steel coupons after short-term marine immersion. *Corrosion: the journal of science and engineering* **71**(7) (2015), 811-818.

3. Young D. *High Temperature Oxidation and Corrosion of Metals*. 2nd edition: Amsterdam, Netherlands: Elsevier Science. 2016.
4. Al-Numan, B. and Cicek V. *Corrosion Chemistry*. Salem, MA, USA: Scrivenger publisher LLC. 2011.
5. Wang Z., Huang W., and Zeng X. Parameters and Surface Performance of Laser Removal of Rust Layer on A3 Steel. *Surface and Coatings Technology* **166** (1) (2003), 10–16.
6. Pierre, R., Roberge, R., and Revie, W. *Corrosion Inspection and Monitoring*. 2012.
7. Waldman, J. *Rust: The Longest War*. New York, USA: Simon & Schuster; Reprint edition. 2015.
8. Wang, F.F.Y. *Laser Material Processing: Material Processing Theory and Practices*. ed. by Boss, M. North-holland publishing company. 2012.
9. Lawrence, J. *Advances in Laser Material Processing: Technology, Research and Application.* Cambridge: Woodhead Publishing. 2017.
10. SPI Lasers (2015) *Laser Cleaning*. Retrieved 25th December 2017, from http://www.spilasers.com/laser-processing-applications/laser-cleaning/.
11. Yilbas, B.S. and Shuja, shahzada Z. *Laser Surface Processing and Model Studies*. 2013.
12. Siatou, A., Charalambous, D., Argyropoulos, V., and Pouli, P. *A Comprehensive Study for the Laser Cleaning of Corrosion Layers due to Environmental Pollution for Metal Objects of Cultural Value : Preliminary Studies on Artificial Corroded Coupons.* Hindawi Publishing corporation. 2006.
13. Fogarassy, E., Geohegen, D., and Stuke, M. *Laser Ablation*. Newnes Australia: Elsevier Science. 2012.
14. Zhenyong, S., Jun, X., and Wengming, Z. *Parameter and Mechanism of Laser Cleaning Rust Deposit on the Steel Surface*. 2002.
15. Koh, Y.S. *Laser Cleaning as a Conservation Technique for Corroded Metal Artifacts*. 2006.
16. Ren Z., Wu C., Chen H., Lu Y., Qiao H., and Hu, T. Mechanism of Laser Derusting and Surface Properties of Low Carbon Steel. *Opto-Electronic Engineering* **44** (12) (2017), 1210–1216.
17. Kane, D.M. *Laser Cleaning*. ed. by Kane, D.M. World Scientific publishing company. 2007.

18. Butcher, E. A green way to clean – Laser cleaning. *Laser Technik Journal.* 9 (11) (2012).
19. Creek, V. *Corrosion Engineering*. Cambridge: Woodhead Publishing. 2014.
20. Sanjeevan P. and Klemm A.J. *A Review of Laser Technique Application in Cleaning Process of Porous Construction Materials*. 2008.
21. Przestacki D., Wietze Otter, H., and Depre, P. *The Cleaning of Superficially Corrosion Metals by CO_2 Laser*. 2006.
22. Adebayo, A. V . Relationship between Graphite Flake Sizes and the Mechanical Properties of Grey Iron. *International Journal of Materials Science and Application.* 2(3) (2013), 94–98.
23. Holtzer M., Gorny, M., and Danta, R. *Microstructure and Properties of Ductile Iron and Compacted Graphite Iron Casting - The Effects of Mold Sand/ Metal Interface Phenomena*. 2015.
24. Varney J., Koch, G., Thompson, N., Moghissi, O., Gould, M., and Payer, J. *NACE International - International Measures of Prevention, Application, and Economics of Corrosion Technologies Study (IMPACT)*. 2016.
25. Renner F.U., Stierle, A., Dosch, H., Kolb, D.M., Lee T-L. and Zegenhagen, J. *Initial corrosion observed on the atomic scale* **439** (9) (2006), 707-710.
26. Koch H.G., Brongers, M.P.H., Thompson, N.G., Virmani, Y.P., and Payer, J.H. *Corrosion Cost and Preventive Strategies in the United States*. Federal Highway Administration, USA. 2002.
27. Kannatey-Asibu, E. *Principles of Laser Material Processing*, 1 edition. New Jersey, USA: Wiley. 2009.
28. Steen, W.M. and Mazumder, J. *Laser Material Processing*. 4th edition London: Springer London. 2010.
29. Siano S. *Principles of Laser Cleaning in Conservation*. M. Schreiner, M. Strlic, R. Salimbeni (eds.): Handbook on the Use of Lasers in Conservation and Conservation Science. 2008.
30. Byskov-Nielsen J., Savolainen J-M. S., Christensen M., and Balling P. Ultra-short pulse laser ablation of metals: threshold fluence, incubation coefficient and ablation rates. *Applied physics A: Materials Science and Processing* **101**(1) (2010), 97-101.
31. Tong Y., Li F., Huang J., Wu X., and Ren X. Simulation and Research on the Laser Removal Mechanism. *International Journal of Non-Linear Science* **23**(3) (2017).

32. Watkins K.G., Curran C., and Lee J.-M. Two New Mechanisms for Laser Cleaning Using Nd:YAG Sources. *Journal of Cultural Heritage.* (2003) 4.
33. ASTM (2017). *ASTM Class 35 Standard Gray Iron Test Bars, as Cast*. Retrieved 30th November 2017, from http://www.matweb.com/search/datasheet_print.aspx?matguid=fcc3101c8cda4cf1b2ce0b1dcde93dd4.
34. Granta Design. *CES 2017 EduPack Software*. 2017.
35. Dhiyaneswaran S. and Amirthagadeswaran, K.S. Comparative study of Disc Brake materials through Computer Aided Engineering. *International Journal of Modern Engineering Research.* (2015) 173-179.
36. Maleque M.A., Dyuti, S., and Rahman, M.M. *Material Selection Method in Design of the Automotive Brake Disc.* 2010.
37. Maluf O., Angeloni, M., Milan, M.T., and Filho B. *Development of materials for automotive disc brakes.* 2004.
38. Yathish K.O., Arun L.R., Kuldeep B., and Muthanna K.P. Performance analysis and material optimization of Disc Brake Using MMC. *International Journal of Innovative Research in Science, Engineering and Technology* **2**(8) (2013), 4101-4108.
39. Ch D., Kiran U.C., and Kumar, V.Y. Design, Analysiss and Manufacturing of Disc Brake Rotor. *International Journal of Engineering Research and Development* **13**(11) (2017), 15-23.
40. Shukla P.P., and Lawrence J. Role of laser beam radiance in different ceramic processing: A two wavelength comparison. *Optics and Laser Technology* **54** (2013) 380 – 388.
41. Shukla P., Lawrence J., Zhang Yu., Understanding Laser-beam brightness: A Review on a New Prospective in Materials Processing, *Optics and Lasers in Engineering*, **75** (2015) 40 – 51.
42. Shukla P.P., and Lawrence J., Identification of Optical Parameters for Determination of Radiance, Journal of Optics, Optical Society of India, **44**(1) (2015) 12-19.
43. Bélisle E., Huang Z., Gheribi A. Scalable Gaussian Process Regression for Prediction of Material Properties. In: Wang H., Sharaf M.A. (eds) Databases Theory and Applications. ADC 2014. Lecture Notes in Computer Science **8506**. (2014) Springer, Cham, https://doi.org/10.1007/978-3-319-08608-8_4.
44. Masoud I.M., Al-Jarrah J.A., and Abu M.T. Manufacturing of Grey Cast Iron Automotive Disc Brake. *Indian Journal of Applied Research* **4**(3) (2014), 131.